Original Research Paper

Addressing the permanent deformation behavior of hot mix asphalt by triaxial cyclic compression testing with cyclic confining pressure

CrossMark

Bernhard Hofko[*]

Institute of Transportation, Vienna University of Technology, Vienna 1040, Austria

ARTICLE INFO

ABSTRACT

Rutting or permanent deformation is one of the major distress modes of hot mix asphalt in the field. Triaxial cycle compression testing (TCCT) is a standardized and scientifically accepted test method to address this distress mode in the lab and to characterize the resistance to permanent deformation. In most labs and according to EN 12697-25, standard TCCTs are carried out with cyclic axial loading and a constant confining pressure. In road pavements on the other hand, dynamic traffic loading due to passing wheels leads to cyclic confining pressure. In order to bring the TCCT closer to reality, the radial reaction and its phase lag to axial loading in standard TCCTs are analyzed and an enhanced TCCT with cyclic confining pressure is introduced. The cyclic confining pressure takes into account the viscoelastic material response by the radial phase lag to axial phase loading. In a subsequent test program, TCCTs with different confining pressure amplitudes were carried out on two hot mix asphalts. Results from standard and enhanced TCCTs were analyzed, compared and discussed. It is shown that the resistance to permanent deformation increases significantly when the viscoelastic material response is taken into account in the TCCT by introducing cyclic confining pressure.

1. Introduction

Besides low-temperature and fatigue cracking, permanent deformation at elevated temperature is a third major distress mode of bituminous bound pavements. Permanent deformation or rutting occurs especially as transverse profile deformations within the wheel paths but can also be seen as longitudinal profile irregularities (Verstraeten, 1995). Rutting is an important deterioration mode since it affects the comfort and safety of road users. Thus, various test methods have been developed to address the permanent deformation behavior of hot mix asphalt (HMA). For comparison of the different HMAs and pavement design the wheel tracking test (WTT) (EN 12697-22, 2007) is commonly used. In this test method a moving wheel stresses a pavement slab at elevated

temperatures for a number of cycles and permanent deformation (i.e. rutting) is recorded. The loading produces a non-homogeneous stress distribution in the slab and thus, results are difficult to interpret when it comes to the rheological behavior of the material (Gabet et al., 2011; Perraton et al., 2011).

An alternative test method to assess the permanent deformation behavior of HMA is the triaxial cyclic compression test (TCCT) with a well-defined external stress state. Research in this field in the 1970s and 1980s (Krass, 1971; Francken, 1977; Jaeger, 1980; Weiland, 1986) was a major source for developing a European standard for TCCTs (EN 12697-25, 2005). Recent studies show the importance of taking into account triaxial behavior with confining pressure (De Visscher et al., 2006; Ebels and Jenkings, 2006; Taherkhani and Collop, 2006; Clec'h et al., 2009; Hofko and Blab, 2010). In the standard TCCT according to EN 12697-25 cylindrical specimens are stressed by a cyclic axial loading in the compressive domain to simulate traffic loading by passing tires. The axial loading can either be shaped as a sinusoidal function or a block-impulse. The confining pressure can either be held constant or cyclic without giving more specific information in the standard. However, most laboratories that have integrated the TCCT on HMA into their test procedures use constant confining pressure, especially since the test control gets even more complex with two independent cyclic loadings.

Research on TCCT with cyclic confining pressure was mainly carried in the area of unbound granular materials (Allen and Thompson, 1974; Brown and Hyde, 1975; Nataatmadia and Parkin, 1989; Zaman et al., 1994; Rondón et al., 2009). While earlier studies (Brown and Hyde, 1975) did not find significant differences in the deformation behavior of unbound material for tests with constant and cyclic confining pressure, more recent studies (e.g. Rondón et al., 2009) showed that differences in permanent deformation occur depending on the ratio of the axial and radial stress amplitude.

The main difference between testing of unbound granular materials and bituminous bound materials (e.g. HMA) is that due to the viscoelastic nature of bituminous bound materials the phase lag between axial loading and radial reaction ($\varphi_{ax,rad}$) must be analyzed and used for cyclic confining pressure to address the viscoelastic material response correctly. Kappl (2004) showed by finite element simulation of a pavement under a passing tire that cyclic axial loading leads to cyclic radial confining pressure within the pavement structure. Thus, the present practice of testing HMA specimens with constant confining pressure is a simplification. Only a small number of studies that work with the TCCT on HMA (von der Decken, 1997; Weise and Wellner, 2008) have been carried out with cyclic confining pressure. The mentioned studies set a constant phase lag between axial loading and radial reaction of 36° for all tested materials at all temperatures and frequencies. Knowing that HMA shows a temperature and frequency dependent viscoelastic behavior, it is questionable whether this constant radial phase lag is correct for all materials, temperatures and frequencies.

2.   Objectives and approach

Since the standard TCCT with constant confining pressure does not represent the state of stress in a pavement structure and the phase lag between axial loading and radial reaction for TCCTs given in literature do not match the common understanding of the theory of viscoelasticity (Findley et al., 1989) that viscoelastic material properties change with temperature and frequency, the main objectives of this study are to measure the radial phase lag $\varphi_{ax,rad}$ between axial loading and radial reaction accurately and to incorporate cyclic confining pressure with a well-defined phase lag $\varphi_{ax,rad}$ to have a more realistic simulation in the TCCT. Results from TCCTs with constant and cyclic confining pressure shall be compared for different mixes. To reach the objectives, the following approach is taken that is also depicted in Fig. 1.

- Carry out standard TCCTs with constant confining pressure, record and analyze the phase lag between axial loading and radial reaction $\varphi_{ax,rad}$ with high precision.
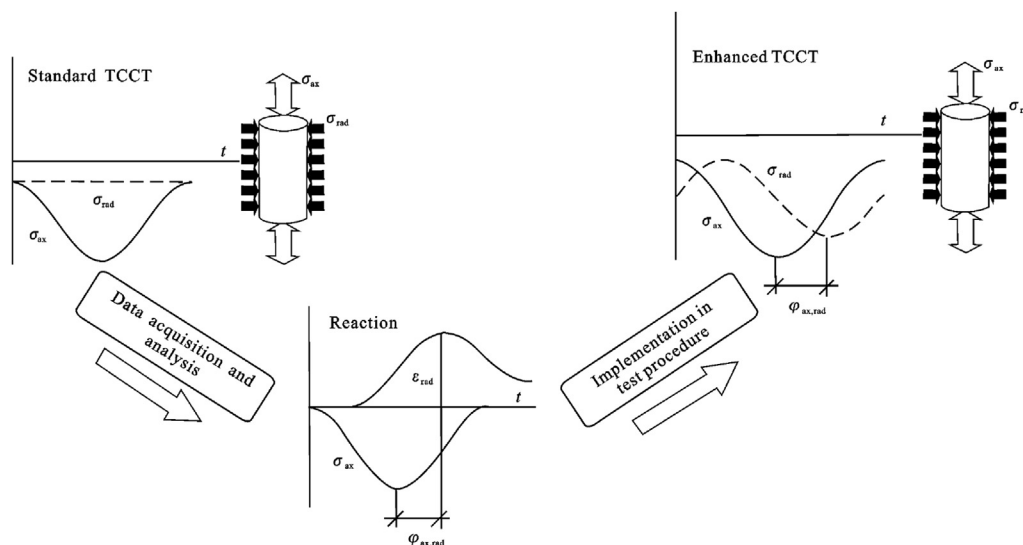

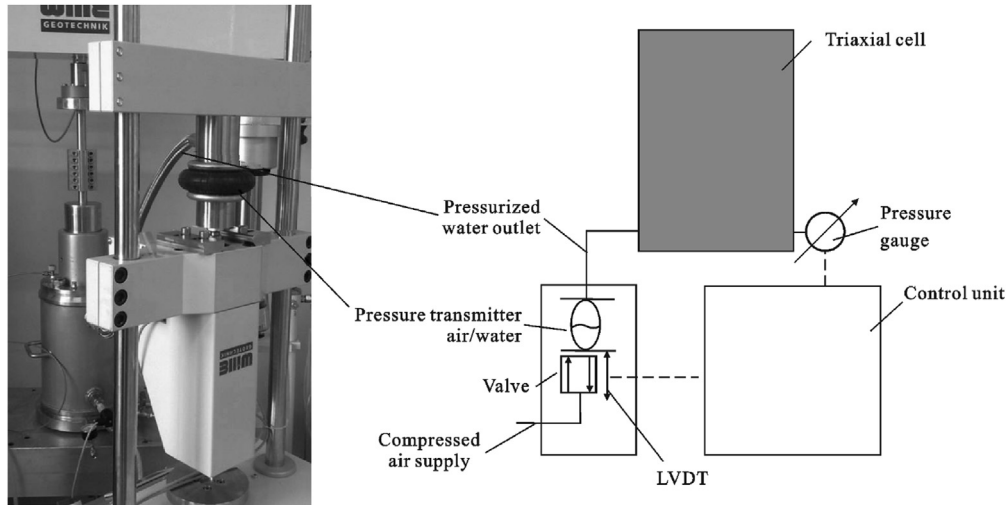Fig. 1 − Approach to introduce cyclic confining pressure in TCCT.

Fig. 2 − **Principle of the pneumatic device to apply cyclic confining pressure.**

- Use the obtained data for the radial phase lag in the further course to incorporate it in an enhanced TCCT with cyclic confining pressure that thus takes into account the visco-elastic material reaction.
- Carry out a test series with the enhanced TCCT with a variation of the amplitude of the cyclic confining pressure to study the impact of the stress deviator on the permanent deformation behavior.
- Analyze, compare and interpret results of standard and enhanced TCCTs run on different HMAs.

Thus, the main goal of this study is to lay the basis for an improved test procedure to address the permanent deformation behavior of HMA. Different from former studies the test will incorporate the actual (measured) radial phase lag of the material to take into account the viscoelastic behavior of HMA. The test can be employed in the future for a more efficient and realistic mix design optimization.

3.   Test equipment

The equipment employed for this study consists of

- A test machine with two circuits, one hydraulic circuit for axial loading including a load cell and a pneumatically driven device for application of static and cyclic confining pressure including a pressure cell
- A temperature chamber to control the test temperature
- A triaxial cell
- Displacement sensors to record axial and radial deformation

When the test machine for triaxial testing was installed in the lab in 2002 it consisted of two hydraulic circuits, one for axial loading and one for radial confinement. Since the hydraulic device for the confining pressure was not able to realize cyclic confining pressure at frequencies higher than 0.1 Hz a new device was developed. The new device (Fig. 2) is based on pneumatics where compressed air is used to activate a stiff membrane. The membrane can be described as a high-end shock absorber also used in heavy goods vehicles (HGVs). It works as a pressure transmitter since it is filled with water and connected to the triaxial cell. The actual control mechanism is a valve that controls the air pressure on the membrane. The more compressed air is put onto the membrane the more water is pressed into the cell. Since the cell is filled with water and the system is water-tight, the pressure within the cell is changed by the volume of water pressed into the cell from the membrane. The triaxial cell is equipped with a pressure gauge. The gauge not only records the pressure, it is also connected to the control unit of the test machine. The control unit drives the valve in the pneumatic device according to the signal of the gauge to reach the target pressure given by the user. An additional linear variable differential transducer (LVDT) below the membrane records the position of the membrane and is a safety device to keep the membrane within safe operation limits.

The user sets a static or cyclic target value for the pressure within the cell and the control unit regulates the pressure with a control frequency of 5 kHz. Thus, exact static or cyclic confining pressure can be realized in a wide range of frequencies and amplitudes. To work correctly, the device needs a compressed air supply of at least 300 l/min and a working pressure of around 800 kPa. For the present study the pneumatic device was optimized to provide amplitudes of the confining pressure of up to 300 kPa at a frequency of up to 3 Hz. To reduce the compressibility of the system which is an important factor to enhance the quality of the driven confining pressure connecting tubes between membrane and cell were kept as short as possible and standard plastic tubes were replaced by tubes reinforced with metal grid.

The triaxial cell (Fig. 3) consists of a base with eight pressure resistant cable outlets, three supporting rods and a top with a guide jacked for the load plunger. De-aeration vents ensure that no air stays within the cell when filled with water before testing. A massive steel jacket is placed around the cell so it can be filled with water and pressurized. The load plates within the cell are configured for cylindrical specimens with a diameter of 100 mm and a height of up to 200 mm. To keep
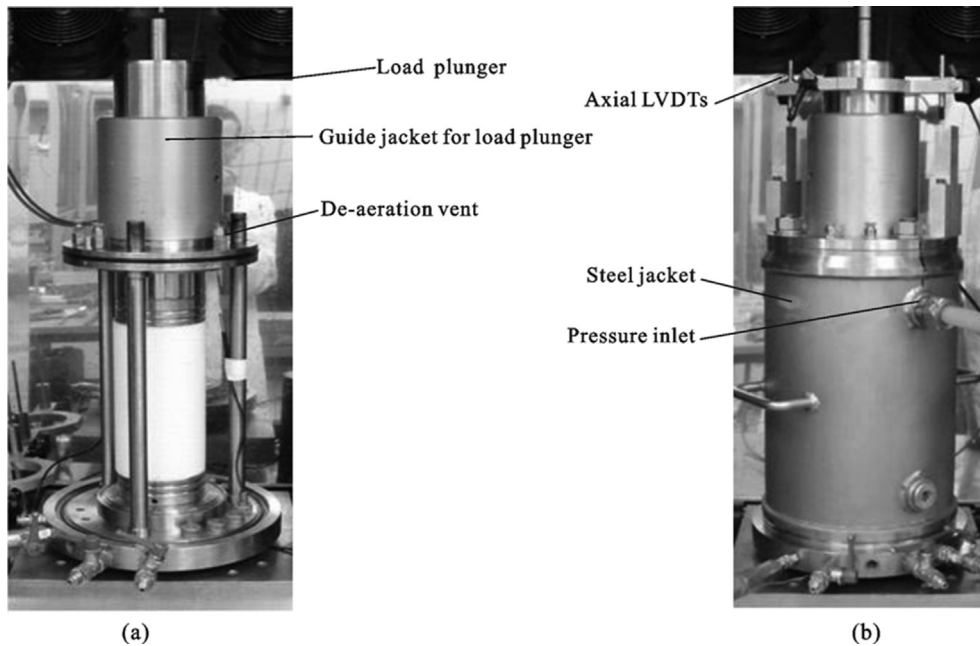
Fig. 3 − Main elements of the triaxial cell.

HMA specimens from the pressurized water, a 0.2 mm latex membrane is placed around the specimen before testing. There is temperature sensor within the triaxial cell to record the water temperature, as well as a sensor that records the air temperature in the temperature chamber.

Also visible in Fig. 3 are two LVDTs placed on top of the load plunger. They measure the axial deformation. For evaluation purposes the mean value (MV) of both signals is used. For the measurement of radial strain, strain gauges are attached directly to the surface of the specimens. One 150 mm strain gauge is laid tightly around the circumference at half height and glued at both of its ends to the specimen. Usually strain gauges are attached to an object over its complete length in order to transfer strain from the object in tension and compression. Since the stiffness of HMA specimens especially at elevated temperatures (in this case 50 °C) is significantly lower than the stiffness of the adhesive, gluing the strain gauges over the complete length would prevent any

deformation within this area. The method used in this study to attach only the end parts of the strain gauge to the specimen is sufficient since radial deformation will only be positive in a purely compressive test. A study by Hofko (2012) compares readings from strain gauges attached only at their end parts to readings from LVDTs and confirms correct measurements of strain gauges in the tensile domain. Fig. 4 shows a detail of a strain gauge attached to an HMA specimen. The figure also contains information on the exact size (15 mm × 20 mm) of the glued area. To ensure that the glued area was the same for every specimen, the area was defined by marking its edges with adhesive tape prior to gluing the strain gauge.

4.   Materials and test program

4.1.   Materials

For the present study an asphalt concrete with a maximum nominal aggregate size of 11 mm (AC 11) was used. The coarse aggregate used for the mixes is a porphyrite (specific gravity: 2830 kg/m^3), a stone commonly used for surface layers in Austria, the filler is powdered limestone (specific gravity: 2700 kg/m^3). Two different binders were used: an unmodified bitumen 70/100 and an SBS-modified binder PmB 25/55−65. The main characteristics of the binders are presented in Table 1. The optimal binder content according to Marshall is 5.3% by mass. This binder content was used for both mixes and the target void content was set to 3.0% by volume for all mixes. The grading curve is shown in Fig. 5. The diagram also contains upper and lower limits for AC 11 mixes according to the national standard (ON B 3580-1, 2009). The maximum density of the unmodified mix was determined to be 2564.0 kg/m^3 and of the modified mix to be 2560.5 kg/m^3.
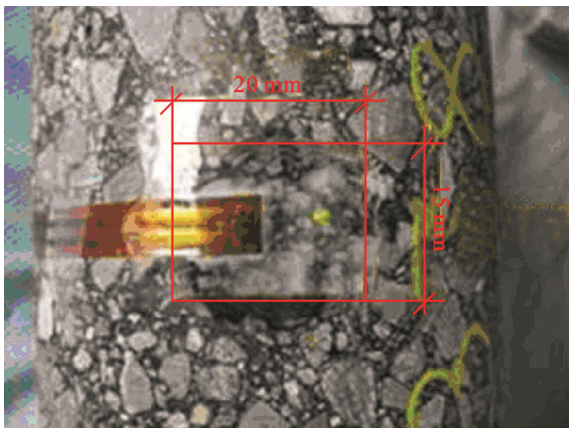

Fig. 4 − End of a strain gauge glued to an HMA specimen.

Table 1 − Characteristics of the employed binders.

Parameter	70/100	PmB 25/55−65
Penetration (1/10 mm)	84	46
Ring and ball (°C)	46.8	73.0
Fraass breaking point (°C)	−17	N/A
SHRP PG (°C)	58−22	>82−16
Mixing temperature (°C)	160	185
Compaction temperature (°C)	135−160	160−185

4.2. Specimen preparation

The complete process of specimen preparation from mixing and compaction to coring and cutting was carried out in accordance to the respective European Standards (EN). The mix was produced in a reverse-rotation compulsory mixer according to EN 12697-35 (2007). The mix drum as well as the mixing device is heated to ensure correct mix and compaction temperatures. The pre-heated aggregates and filler are mixed for 1 min before the pre-heated bitumen is added to the mix. Aggregates, filler and bitumen are mixed for an additional 3 min. After the mixing process the material is compacted in a segment roller compactor according to EN 12697-33 (2007). Slabs compacted by the device have a base area of 50 cm × 26 cm and a variable height of up to 22 cm. The radius of the segment of 55 cm corresponds to the size of standard roller compactors used in the field. It was shown by Hunter et al., 2004) that this compaction method reproduces the compaction in the field in the best way of all compaction methods given by European Standards at this time.

The slabs were compacted to a target height of 13.0 cm in a displacement-controlled way. The complete slab was compacted in two layers hot on hot. Single-layered compaction leads to a large scatter of the density between upper and lower parts of the slab (Hoeflinger, 2006). Since the maximum density is known as well as the target content of air voids, the target unit weight can be derived. The target unit weight and the target volume of the slab define the necessary mass of the material for compaction.

From each slab, four specimens were cored out with a diameter of 100 mm (Fig. 6). The obtained specimens were then cut to a height of 200 mm. Compared to the direction of the compaction force, the direction of coring is orthogonal to the compaction. The reason for this specimen orientation is
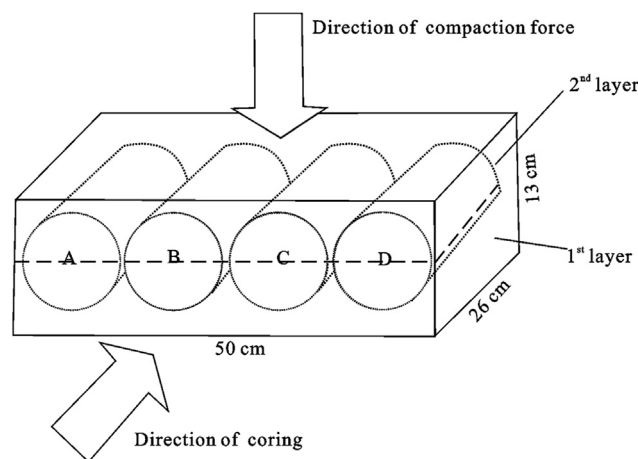

Fig. 6 − Principle of specimen direction within HMA slab.

mainly practical. If the specimens were cored out so that the height of the specimen is in direction of the compaction force, the slab would have to be at least 22 cm in height. This would almost double the mass of the slab to around 80 kg and thus the slabs would be hard to handle in the lab. Of course, the stress/strain situation in a pavement is simulated better when the specimens are cored so that its height is in direction of the compaction force. Before the specimens were finally tested they were stored at the test temperature for at least 4 h but no longer than 7 h.

4.3. Test program

The test temperature was set to 50 °C, the sinusoidal test frequency was set to 3 Hz. All tests were run for 25,000 load cycles. To introduce an enhanced TCCT with cyclic confining pressure, the radial phase lag $\varphi_{ax,rad}$ between axial loading and radial deformation was determined in standard TCCTs. To study the impact of the amplitude of the confining pressure, enhanced TCCTs were carried out at three different amplitudes on three specimens for each amplitude. Table 2 shows the layout of the test program. The table presents the lower and upper value of the axial stress ($\sigma_{ax,l}$ and $\sigma_{ax,u}$) and the radial confining stress ($\sigma_{rad,l}$ and $\sigma_{rad,u}$). The lowest radial stress amplitude (i.e. the difference between upper and lower stress value) is 50 kPa, the other two are set to be 75 kPa and 100 kPa.
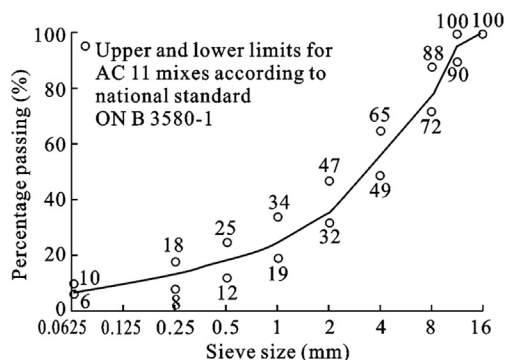
5. Data evaluation

For the analysis of the periodic (sinusoidal) component of the test data a regression analysis was employed with the following function

$$f(t) = a_1 + a_2 \sin(2\pi f t + a_3) + a_4 t \tag{1}$$

where $f(t)$ is regression function of the periodic component of test data, a_1 is vertical offset of the regression function, a_2 is amplitude of the regression function, a_3 is phase lag of the regression function, a_4 is gradient of the linear term of the regression function, f is frequency (Hz), t is time (s).


Fig. 5 − Grading curve of AC 11.

Table 2 − Test program.

Test conditions	Type	$\sigma_{ax,l}$ (kPa)	$\sigma_{ax,u}$ (kPa)	$\sigma_{rad,l}$ (kPa)	$\sigma_{rad,u}$ (kPa)
50 °C, 3 Hz, 25,000 load cycles	Standard	150	750	150	150
	Enhanced	150	750	150	250
		150	750	150	300
		150	750	150	350

For the regression analysis the test data is split into individual packets of three oscillations. For each of these packets a regression analysis with the function shown above is carried out. The reason to take three oscillations for each analysis is to achieve a more robust and stable evaluation routine. The sum of square errors between test data and approximation function is aimed to become minimal by systematically varying the parameters of the function. The quality of the approximation is described by the coefficient of determination R^2. If R^2 is below 0.95, the oscillation packet is omitted from the subsequent data analysis since the deviation between approximation function and test data is considered too large. This regression is carried out for data from the axial load cell, the mean value of the two axial LVDTs, the data from the radial strain gauge and from the pressure cell recording confining pressure. The analytical functions of the periodic component are then used to calculate extreme values and from that the time lag between different sensor data to obtain phase lags between axial loading and radial deformation for all applied load cycles.

The non-periodic, axial deformation component for data from tests in the compressive domain can be described by a creep curve to assess the permanent deformation behavior. To determine the permanent axial strain from the test data, the minimal axial strain value from the analysis of the periodic component of each load cycle is used to create the creep curve. Creep curves obtained from TCCTs according to EN 12697-25 can be divided into three different phases (Fig. 7)

- The primary phase 1: within the first phase of a TCCT a certain amount of recompaction leads to decreasing slope of the curve with increasing number of load cycles.
- The secondary phase 2: the main phase of the TCCT is characterized by a quasi-constant slope of the curve.
- The third phase 3: usually the standard TCCT does not reach this state where the deterioration of the specimen
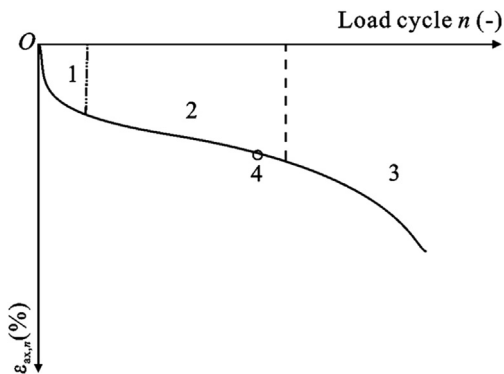
Fig. 7 − Example of a creep curve.

leads to an increase of the slope of the curve with increasing number of load cycles.

The axial strain is determined for the complete test and presented in a load-cycle-strain-diagram with linear scale for both axes. The secondary creep phase with a quasi-constant incline of the creep curve is approximated by the following linear function by using the method of least squares

$$\varepsilon_{ax}(n) = A_1 + B_1 n \tag{2}$$

where $\varepsilon_{ax}(n)$ is approximated function for permanent axial strain at the load cycle n (%), A_1 is regression parameter describing the intersection of the approximation function with the y-axis (offset) (%), B_1 is regression parameter describing the incline of the approximation function (%/load cycle), n is load cycle.

To define the secondary quasi-linear phase, the linear regression is used to approximate the creep curve starting between load cycles 1000 and 20,000. If the coefficient of determination R^2 is below 0.98 for this range of load cycles, the lower load cycle limit for linear regression is increased in steps of 500 until R^2 is above 0.98. For all tests carried out in this study the load cycle range for the secondary phase was from load cycle 5000 to 20,000.

The creep rate f_c is determined as the incline B_1 (%/load cycle) of the linear function in micrometers per meter (i.e. μstrain) per load cycle

$$f_c = 10^4 B_1 \tag{3}$$

where f_c is used to determine the resistance of a specimen to permanent deformation. The smaller its absolute value, the smaller the increase of permanent deformation vs. load cycles. Thus, a smaller absolute value of f_c means that the resistance to permanent deformation is higher.

In addition the permanent deformation is also described by the total axial strain $\varepsilon_{ax,tot}$ after 10,000 load cycles. Since both, the axial and radial deformation is recorded for all tests, two strain components of the total axial strain, the volumetric and deviatoric strain component can be determined as follows: a cylindrical specimen shall have an initial height h_0, an initial diameter of d_0 and thus an initial volume of

$$V_0 = \frac{\pi d_0^2}{4} h_0 \tag{4}$$

The change in height Δh_n and in diameter Δd_n with each load cycle n results in the volume

$$V(n) = \frac{\pi (d_0 + \Delta d_n)^2}{4}(h_0 - \Delta h_n) \tag{5}$$

If the pure deviatoric part of the deformation (without any change in volume) shall be derived, $V(n)$ in the formula above has to be substituted by V_0 and solved for Δh_n which then becomes $\Delta h_{n,dev}$

$$\Delta h_{n,dev}(n) = h_0 - \frac{4V_0}{\pi (d_0 + \Delta d_n)^2} \tag{6}$$

This change in height can be converted to an axial strain component by dividing it by the initial height h_0. If the total axial strain is referred to as $\varepsilon_{ax,tot}$ then the deviatoric and volumetric strain component can be defined as follows

$$\varepsilon_{\text{ax,dev}}(n) = \frac{\Delta h_{n,\text{dev}}(n)}{h_0} \tag{7}$$

$$\varepsilon_{\text{ax,vol}}(n) = \varepsilon_{\text{ax,tot}}(n) - \varepsilon_{\text{ax,dev}}(n) \tag{8}$$

where $\varepsilon_{\text{ax,vol}}$ is volumetric part of the axial strain, $\varepsilon_{\text{ax,dev}}$ is deviatoric part of the axial strain.

6.   Results and interpretation

6.1.   Analysis of phase lag $\varphi_{ax,rad}$

As a first step standard TCCTs with constant confining pressure were carried out on three specimens for the two mixes. Test data was evaluated in terms of phase lag $\varphi_{\text{ax,rad}}$ between axial loading and radial deformation. Fig. 8 presents an example of the evolution of $\varphi_{\text{ax,rad}}$ vs. the number of load cycles for one specimen. For the evaluation of the phase lag, data from load cycle 500 on were considered since there is a strong change in the phase lag within the first 500 load cycles due to recompaction in the first phase of a TCCT. The gray lines show the actual test data, the black line the mean value of all data and the dashed black lines the 95% confidence interval. The confidence interval shows a scattering of around 6.

For the further evaluation of $\varphi_{\text{ax,rad}}$ data from the three single standard TCCTs carried out for each mix were merged and statistically analyzed. Table 3 shows mean values of $\varphi_{\text{ax,rad}}$ as well as the 2.5% and 97.5% quantiles for both mixes. The scattering of $\varphi_{\text{ax,rad}}$ in terms of the 95% confidence interval is 12.8° for the unmodified AC 11 and lower (4.5°) for the modified AC 11. Also, the mean value of the modified mix (19.1°) is about 2° lower than the mean value of the unmodified mix. This is caused by the SBS modification of the binder which leads to a higher elastic component especially at elevated temperatures compared to unmodified bitumen. The mean values of $\varphi_{\text{ax,rad}}$ serve as input values for the enhanced TCCTs to set the phase lag between axial loading and radial confining pressure and thus take into account the viscoelastic material response in the enhanced TCCT.
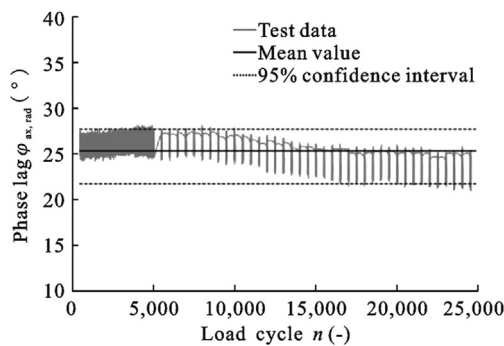

Fig. 8 − Evolution of phase lag between axial loading and radial deformation $\varphi_{\text{ax,rad}}$ vs. number of load cycles for one specimen of AC 11 70/100 in standard TCCT ($T_{\text{test}} = 50$ °C, $f = 3$ Hz, $\sigma_{\text{ax,l}} = 150$ kPa, $\sigma_{\text{ax,u}} = 750$ kPa, $\sigma_{\text{rad,l}} = \sigma_{\text{rad,u}} = 150$ kPa).

Table 3 − Phase lags $\varphi_{\text{ax,rad}}$ derived from standard TCCTs.

Type	AC 11 70/100	AC 11 PmB 25/55−65
2.5% quantile	14.8°	16.4°
Mean value of 3 samples	21.2°	19.1°
97.5% quantile	27.6°	20.9°

Note: $T_{\text{test}} = 50$ °C, $f = 3$ Hz, $\sigma_{\text{ax,l}} = 150$ kPa, $\sigma_{\text{ax,u}} = 750$ kPa, $\sigma_{\text{rad,l}} = \sigma_{\text{rad,u}} = 150$ kPa.

6.2.   Analysis of TCCTs with cyclic confining pressure

Fig. 9 gives an example of the recorded test data from an enhanced TCCT. It shows three oscillations of the axial stress on the top (from the axial load cell), the confining pressure in the middle (from the pressure gauge) and the resulting radial deformation on the bottom (from the strain gauge). The solid vertical line indicates a minimum of the axial loading, and the dashed line indicates a minimum of the confining pressure. This demonstrates that the test machine is working correctly and the confining pressure actually lags behind the axial loading as set by the user. The extreme values of the confining pressure also coincide with the extreme values of the radial deformation. This shows that the chosen phase lag for the confining pressure taken from standard TCCTs is correct and accounts for the viscoelastic material response.

From each mix, three specimens were tested at each test condition. The air void content of the successfully tested specimens is listed in Table 4 for AC 11 70/100 and in Table 5 for AC 11 PmB 25/55−65.

All tests were run at 50 °C and 3 Hz for 25,000 load cycles and an axial stress amplitude of 150 kPa−750 kPa. Different from the standard TCCT according to EN 12697-25 the radial stress amplitude is varied in three ranges. The test procedure starts from a hydrostatic state of stress on the low level where both the radial and axial stress are at the same level at 150 kPa. This pre-loading phase is held constant for 120 s. Then, the axial sinusoidal loading starts and with a well-defined time lag (i.e. the phase lag $\varphi_{\text{ax,rad}}$) the confining pressure starts to oscillate sinusoidally as well. The stress applied to the specimen for each point in time t can be given as

$$\sigma_{\text{dev}}(t) = \sigma_{\text{ax,m}} + \sigma_{\text{ax,a}} \sin(2\pi t) - \left[\sigma_{\text{rad,m}} + \sigma_{\text{rad,a}} \sin\left(2\pi t - \varphi_{\text{ax,rad}}\right)\right] \tag{9}$$

where σ_{dev} is stress deviator, $\sigma_{\text{ax,m}}$ is mean axial stress, $\sigma_{\text{ax,a}}$ is axial stress amplitude, $\sigma_{\text{rad,m}}$ is mean radial stress, $\sigma_{\text{rad,a}}$ is radial stress amplitude.

The expression above is also valid for standard TCCTs where the mean radial stress is set to 150 kPa and the radial stress amplitude is set to 0. One objective of the following investigation is to compare results from standard and enhanced TCCTs. To carry out this investigation, the stress applied on the specimen within one load cycle must be calculated to be able to compare different test conditions. For this reason Eq. (9) can be integrated over one oscillation period $T_p = 2\pi/f$, or since all tests were run at the same frequency over 2π. This number is equal to an impetus and is independent of the radial phase lag $\varphi_{\text{ax,rad}}$. For the lowest radial stress amplitude from 150 kPa to 250 kPa a value of 500π results from the integration, for the medium amplitude of 450π and for the

(a) Axial stress

(b) Confining pressure

(c) Radial deformation

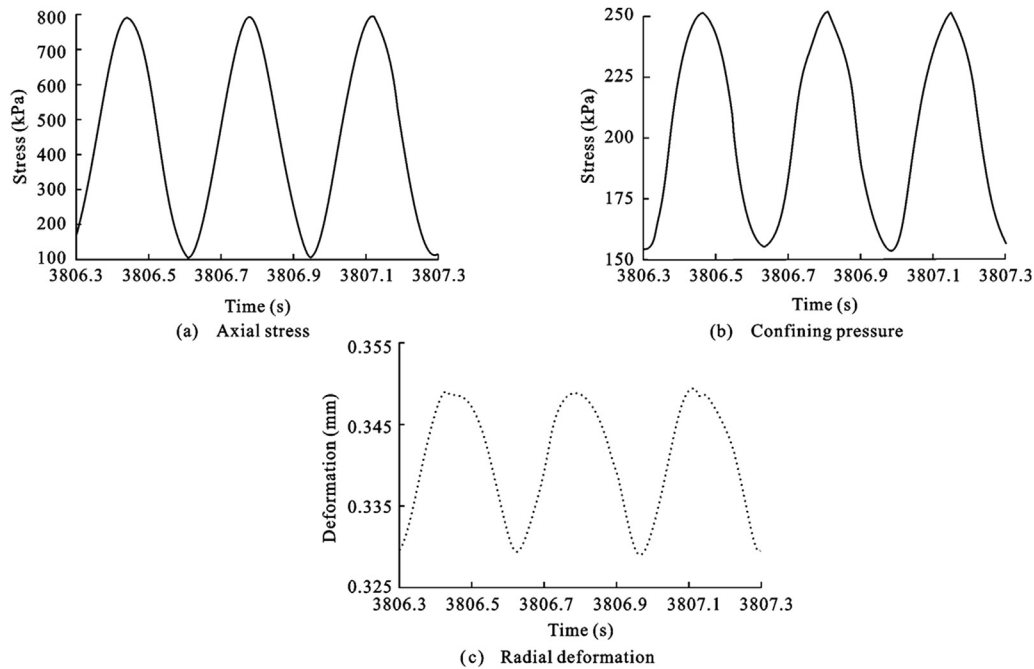**Fig. 9 – Example of recorded test data from enhanced TCCT for one specimen of AC 11 PmB 25/55–65 with cyclic confining pressure (T_{test} = 50 °C, f = 3 Hz, $\sigma_{ax,l}$ = 150 kPa, $\sigma_{ax,u}$ = 750 kPa, $\sigma_{rad,l}$ = 150 kPa, $\sigma_{rad,u}$ = 250 kPa).**

highest amplitude of 400π. The value for the standard TCCT with constant confining pressure is 600π.

For the **AC 11 70/100** the phase lag between axial loading and radial confining pressure was set according to the results from standard TCCTs listed in Table 3. To check how well the given phase lag was controlled by the test machine throughout the test, the actual phase lag between axial loading and confining pressure was analyzed with regard to the time shift between both signals for each test and load cycle. Fig. 10 shows these results for the three different test conditions. The diagrams show the mean value as well as the 95% confidence interval (light gray bar 2.5% quantile to mean value, dark gray bar mean value to 97.5% quantile) of the deviations between given and actual phase lag. At the lowest radial stress amplitude (Fig. 10 (a)) all specimens were tested successfully. The worst deviation between given and actual phase lag is 9.6° or 5.3% (the basis is 180° since this represents the largest deviation possible). 97.5% of the test data show a lower deviation. At the second amplitude (150 kPa–300 kPa, Fig. 10 (b)) only one out of three tests ran successfully. The maximum deviation is similar to the tests with the lowest amplitude. Since the deviations were higher than expected,

the test machine was optimized once more by adapting the PID (Proportional-Integral-Derivative) control of the pneumatic device responsible for the confining pressure. After this optimization the test series was continued. For the largest radial amplitude (150 kPa–350 kPa, Fig. 10 (c)) two specimens were tested successfully. The error of the actual to the given radial phase lag is below 2.7° or 1.5% in 97.5 out of 100 cases.

For the further analysis, it is of great interest, how the different radial amplitudes affect the results of TCCTs in terms of resistance to permanent deformation and if there are any differences between standard and enhanced TCCTs. For this reason, a number of diagrams compare the stress deviator to various parameters which describe the deformation behavior. The stress deviator multiplied by π is congruent to the impetus put into the specimen at each load cycle and thus a proper parameter to compare different test conditions. Each diagram in Figs. 11, 12, 14 and 15 contains data from each single enhanced TCCT, highlighted in gray together with a linear regression. In addition, a 95% confidence interval was place around the linear regression. The confidence interval was derived by computing the relative error RE between each data point and the linear regression. In the following, the 2.5%

Table 4 – Air void content of all successfully tested specimens for AC 11 70/100.

AC 11 70/100	Radial stress levels ($\sigma_{rad,l}$–$\sigma_{rad,u}$) (kPa)			
	150–150	150–250	150–300	150–350
Specimen #1	3.2	3.3	2.7	3.5
Specimen #2	2.8	2.7	N/A	3.0
Specimen #3	2.7	2.9	N/A	N/A
Mean value	2.9	3.0	2.7	3.3
Standard deviation	0.3	0.3	N/A	0.4

Table 5 – Air void content of all successfully tested specimens for AC 11 PmB 25/55–65.

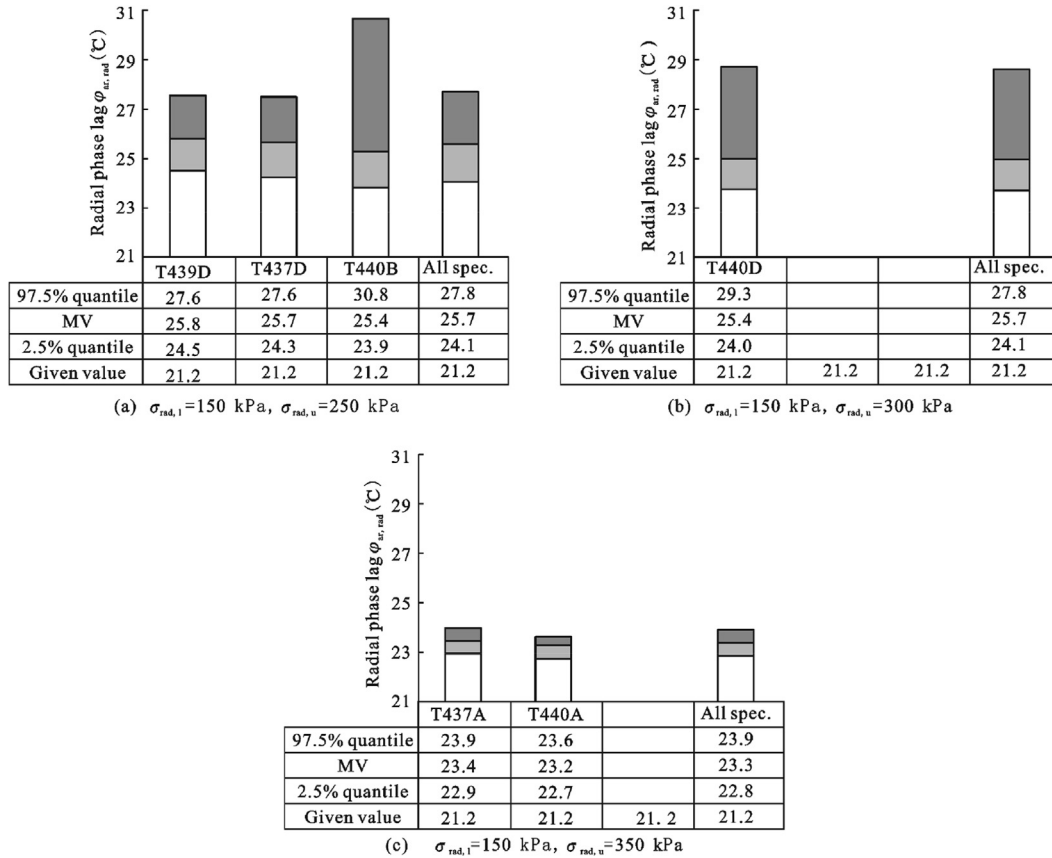| AC 11 PmB 25/55–65	Radial stress levels ($\sigma_{rad,l}$–$\sigma_{rad,u}$) (kPa)			
	150–150	150–250	150–300	150–350
Specimen #1	3.4	2.5	3.2	3.3
Specimen #2	3.0	2.4	3.0	2.5
Specimen #3	3.1	2.3	N/A	2.6
Mean value	3.2	2.4	3.1	2.8
Standard deviation	0.2	0.1	0.1	0.4

Fig. 10 − **Phase lag between axial loading and radial confining pressure induced by the test machine vs. given value from the standard TCCTs for AC 11 70/100 (binder content = 5.3% by mass, target void content = 3.0% by volume) with a confining pressure of 150−250 kPa (a), 150−300 kPa (b) and 150−350 kPa (c) ($T_{\text{test}} = 50\ ^{\circ}$C, $f = 3$ Hz, $\sigma_{\text{ax,l}} = 150$ kPa, $\sigma_{\text{ax,u}} = 750$ kPa).**

and 97.5% quantiles were obtained for this relative error. These quantile values were then used to create the two confidence interval lines from the linear regression as follows

$$f_1(x) = (ax + b)(1 + RE_{2.5\%}) \tag{10}$$

$$f_2(x) = (ax + b)(1 + RE_{97.5\%}) \tag{11}$$

where a is slope of the linear regression, b is Y-intercept of the linear regression, $RE_{2.5\%}$ is 2.5% quantile of the relative error, $RE_{97.5\%}$ is 97.5% quantile of the relative error.

Data from standard TCCTs are also shown in the diagrams marked in black to compare enhanced TCCT to standard TCCT results.

Fig. 11 shows a compilation of all test results from enhanced TCCTs in terms of axial strain at load cycle 10,000 vs. the stress deviator. Fig. 11 (a) shows the total axial strain. There is a decreasing trend with increasing stress deviator showing that a higher stress level leads to more deformation. Although the 95% confidence interval is quite large, the standard TCCT results in significantly more total axial strain (−3.5% vs. −2.8% from enhanced TCCTs) at comparable stress levels. Thus, specimens tested in the standard TCCT setup suffer 25% more axial strain than those tested under enhanced conditions at comparable stresses. This benefit of

the enhanced TCCT can be explained by the fact that the viscoelastic material response of the material is taken into account by the radial phase lag. When the volumetric and deviatoric part of the axial strain are taken into consideration, it can be analyzed which strain component is affected by taking into consideration the viscoelastic material response. Fig. 11 (b) and (c) presents the situation for the volumetric and deviatoric part of the axial strain. The scatter of results is quite large. It seems that the axial volumetric strain hardly depends on the stress level. This may be due to the high degree of compaction (3.0% by volume voids). The standard TCCTs (MV of $\varepsilon_{\text{ax,vol}}$ −2.2%) results in 32% more volumetric deformation than the prediction from enhanced TCCTs (−1.7%). From Fig. 11(c) it is clear that the impact of the stress deviator on the deviatoric strain component is more significant. The standard TCCT results in a MV of $\varepsilon_{\text{ax,dev}}$ of −1.7% compared to a value of −1.3% from enhanced TCCT at the same stress level. The material exhibits 21% less deviatoric strain when tested with the enhanced test setup. It can therefore be stated that this mix reacts in a positive way (i.e. shows a better resistance to permanent deformation) when the viscoelastic material reaction is taken into account.

The same analysis is also provided for the creep rate f_c in Fig. 12. The situation here is more significant since the scatter
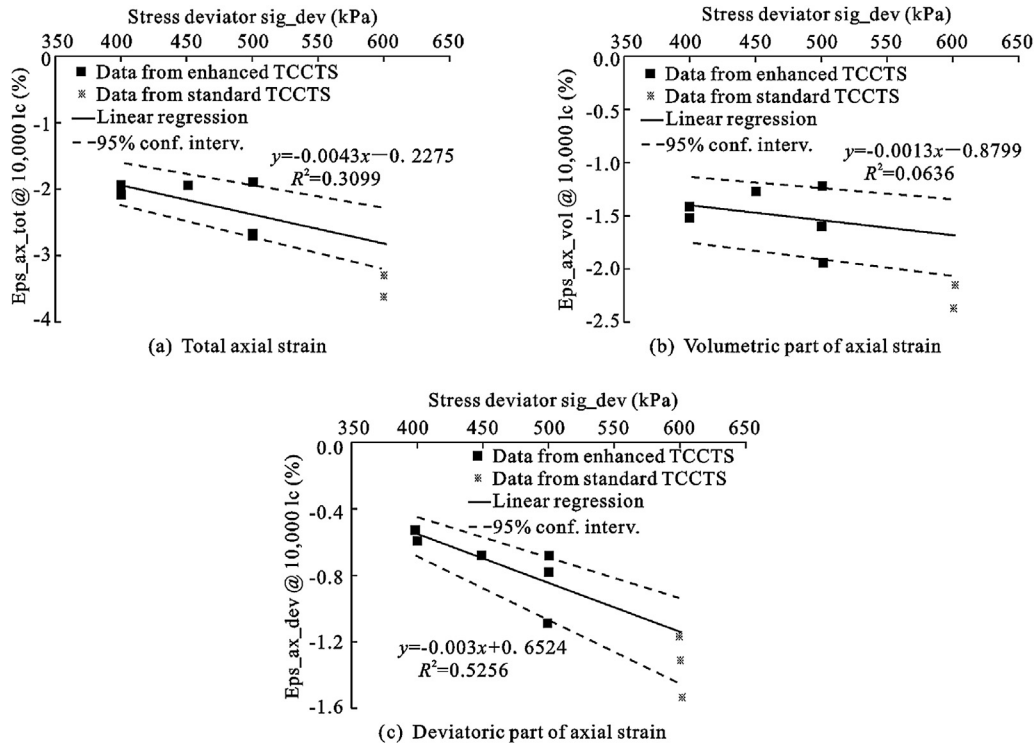
Fig. 11 – Total axial strain, volumetric axial strain and deviatoric axial strain at load cycle 10,000 for AC 11 70/100 (binder content 5.3% by mass, target void content 3.0% by volume) at different stress deviators from standard and enhanced TCCTs ($T_{\text{test}} = 50\ ^{\circ}$C, $f = 3$ Hz).

of results is less severe. The creep rate decreases with increasing stress deviator, showing – analogue to the total axial strain – that the material exhibits more permanent deformation when the stress level is increased. Again, it is obvious that the material contains a potential of better resistance to permanent deformation when the viscoelastic material reaction is considered in the TCCT. For the creep rate, standard TCCTs result in MV of -0.301 μstrain/load cycle, enhanced TCCTs at the same stress level in MV of -0.245 μstrain/load cycle (-19%).

For the AC 11 PmB 25/55–65 the standard TCCTs resulted in MV of the radial phase lag of 19.1° (Table 3). To make sure that the given phase lag was controlled correctly throughout the

Fig. 12 – Creep rate f_c in μstrain/load cycle for AC 11 70/100 (binder content 5.3% by mass, target void content 3.0% by volume) at different stress deviators from standard and enhanced TCCTs ($T_{\text{test}} = 50\ ^{\circ}$C, $f = 3$ Hz).

test, the actual phase lag between axial and radial stress was analyzed with regard to the time shift between both signals for each test and load cycle. Fig. 13 presents these results for the three different radial amplitudes. The largest deviation between given and actual radial phase lag occurred for the lowest radial amplitude of 150 kPa–250 kPa (Fig. 13 (a)) with a mean value of 23.4° instead of 19.1°. The error between actual and given phase lag could be reduced to 4.3° or 2.4% in the worst case.

Fig. 14 (a) shows the total axial strain $\varepsilon_{\text{ax,tot}}$ at load cycle 10,000. There is a clear linear link between the stress deviator and the permanent deformation in the enhanced TCCTs. A stronger radial confinement (i.e. higher amplitudes of the confining pressure) results in less permanent axial deformation. When the results of the standard TCCT are compared to the results of the enhanced test, it becomes obvious that two of three data points are out of the 95% confidence interval. There seems to be a significant difference between both test types. The material suffers more axial strain when the radial confining pressure is held constant. The MV of $\varepsilon_{\text{ax,tot}}$ from standard TCCTs is -2.4% compared to -2.2% from the enhanced TCCTs at the same stress level. This shows that by considering the viscoelastic materials response of the mix in the test procedure, the material exhibits 10% less axial strain. When the volumetric and deviatoric part of the axial strain $\varepsilon_{\text{ax,vol}}$ and $\varepsilon_{\text{ax,dev}}$ are taken into account, it can be investigated where the origin of this benefit lies. Fig. 14 (b) shows the volumetric axial strain. In this case, the MV of the test data from standard TCCTs is -1.3% compared to a predicted -1.5% from the regression of the enhanced TCCTs. An enhanced
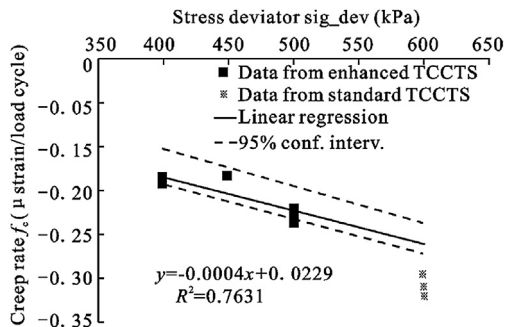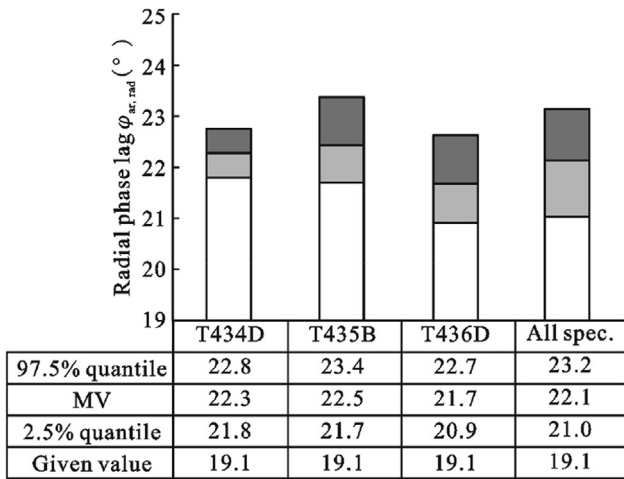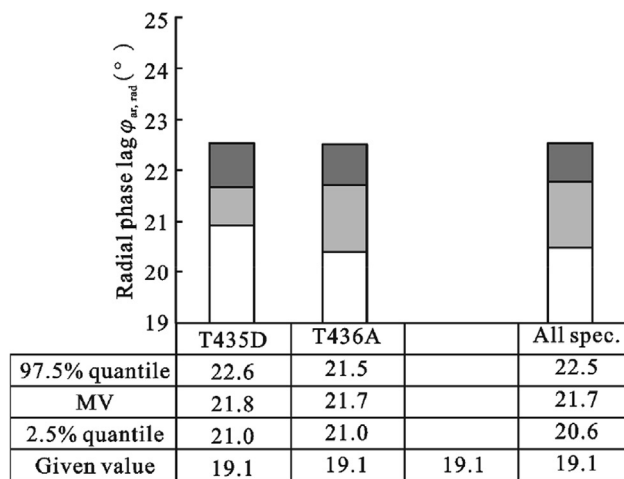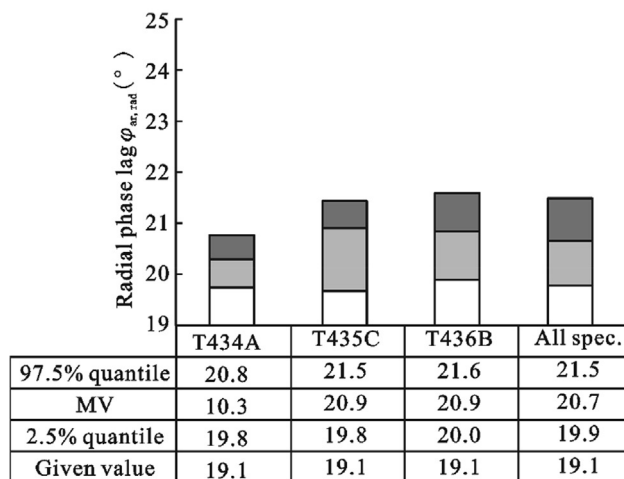
(a) $\sigma_{\mathrm{rad,l}}=150$ kPa, $\sigma_{\mathrm{rad,u}}=250$ kPa

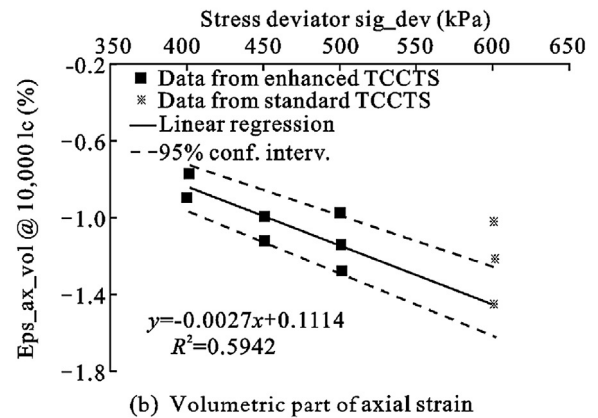(b) $\sigma_{\mathrm{rad,l}}=150$ kPa, $\sigma_{\mathrm{rad,u}}=300$ kPa

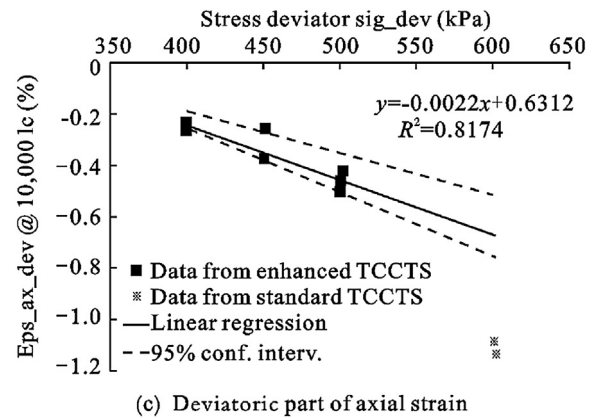(c) $\sigma_{\mathrm{rad,l}}=150$ kPa, $\sigma_{\mathrm{rad,u}}=350$ kPa

Fig. 13 − Phase lag between axial loading and radial confining pressure induced by the test machine vs. given value from the standard TCCTs for AC 11 PmB 25/55−65 (binder content 5.3% by mass, target void content 3.0% by volume) with a confining pressure ($T_{\mathrm{test}} = 50$ °C, $f = 3$ Hz, $\sigma_{\mathrm{ax,l}} = 150$ kPa, $\sigma_{\mathrm{ax,u}} = 750$ kPa).
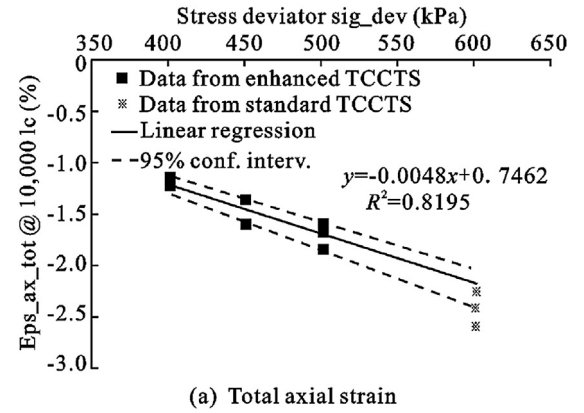
(a) Total axial strain

(b) Volumetric part of axial strain

(c) Deviatoric part of axial strain

Fig. 14 − Total axial strain, volumetric axial strain and deviatoric axial strain at load cycle 10,000 for AC 11 PmB 25/55−65 (binder content is 5.3% by mass, target void content is 3.0% by volume) at different stress deviators from standard and enhanced TCCTs ($T_{\mathrm{test}} = 50$ °C, $f = 3$ Hz).

TCCT would produce 16% more volumetric strain at comparable stress levels. Looking at the deviatoric axial strain in Fig. 14 (c), the enhanced TCCTs exhibit significantly less deformation: −1.1% (standard TCCT) vs. −0.7% (prediction from enhanced TCCT) or 40% less deviatoric strain. This shows that the reason for the better performance of the material in the enhanced TCCT is due to the fact that far less deviatoric strain is activated.
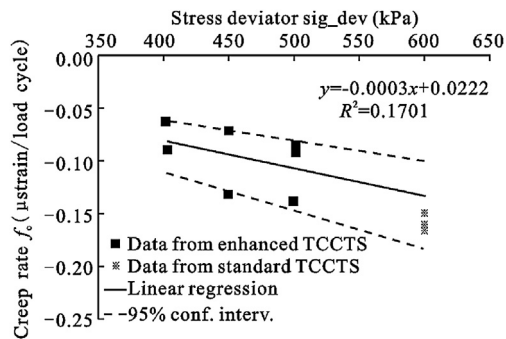
Fig. 15 – Creep rate f_c in μstrain/load cycle for AC 11 PmB 25/55–65 (binder content = 5.3% by mass, target void content = 3.0% by volume) at different stress deviators from standard and enhanced TCCTs (T_{test} = 50 °C, f = 3 Hz).

Fig. 15 shows the interrelation between the stress deviator and creep rate f_c describing the creep curve from TCCTs. The 95% confidence interval covers a large area around the regression. Still, there is a decreasing tendency with increasing stress deviator. The MV of f_c for the standard TCCTs is −0.158 μstrain/load cycle compared to a predicted value of −0.132 μstrain/load cycle with the linear regression for the data of enhanced TCCTs at the same stress level. This means that an enhanced TCCT at the same stress level as the standard TCCT would produce a 16% lower creep rate. It shows again that there is a benefit in the permanent deformation behavior of the mix if the viscoelastic material response is taken into consideration.

7. Conclusions

Within the study presented in this paper cyclic confining pressure was introduced into the TCCT to simulate the state of stress that occurs in the field in a more realistic way. The results of standard and enhanced TCCTs are compared and interpreted. The main findings are summarized below.

- The pneumatic device developed for TCCTs with cyclic confining pressure was successfully employed in the study for the first time. After preliminary problems with the control of the target phase lag between axial loading and confining pressure (deviations of up to 9.6° between given and actual phase lag), a second optimization of the device was carried out. After that the error of the actual to given phase lag was around or below 4°. This is satisfactory when it is kept in mind that a scattering of $\varphi_{ax,rad}$ of around 6° occurs when measured on specimens in standard TCCTs.
- For both tested mixes, an AC 11 with unmodified bitumen 70/100 and SBS-modified binder 25/55–65 the total axial strain $\varepsilon_{ax,tot}$ after 10,000 load cycles decreases when the enhanced TCCT with cyclic confining pressure is compared to the standard TCCT with constant confining pressure at comparable stress levels. The unmodified mix suffers from 25% more, the modified mix from 10% more axial strain in the standard TCCT.

- The volumetric strain component $\varepsilon_{ax,vol}$ shows different results. While specimens from the unmodified mix exhibit 32% more volumetric strain in the standard TCCT, specimens from the modified mix show 16% less volumetric strain in the standard TCCT. One reason for these inconclusive results could be the high degree of compaction. All slabs were compacted to a target void content of 3.0% by volume.
- For the deviatoric strain component $\varepsilon_{ax,dev}$ the results are more conclusive. For both mixes, specimens in the standard TCCT exhibit more deviatoric strain after 10,000 load cycles. The unmodified mix shows 21% more, the modified mix 40% more deviatoric strain. These findings can be explained by the fact that the viscoelastic material response is taken into consideration in the enhanced TCCT. This means that the maximum confining pressure is activated at the point of maximum radial deformation. Thus, the deviatoric strain component, which is the component responsible for changes in the shape of a specimen, decreases.
- The creep rate f_c is the benchmark parameter for the assessment of the resistance to permanent deformation in the European Standard for production classification of HMA. The quality of a mix is defined by classes of the creep rate ($0.0 \leq f_c < 0.2$, $0.2 \leq f_c < 0.4$, $0.4 \leq f_c < 0.6$, …). f_c decreased for both mixes when they were tested in the enhanced TCCT. The unmodified mix shows a 19% lower, the modified mix a 16% lower creep rate compared to standard TCCT results.

Since only a limited number of mixes and specimens was tested in the test program for this study, the significance of the findings is yet limited. Still, the potential of enhancing the TCCT not only by introducing cyclic confining pressure but especially by taking into consideration the viscoelastic material response with the radial phase lag $\varphi_{ax,rad}$ for the cyclic confining pressure could be shown by the investigation. Specimens tested in the enhanced TCCTs show a significantly higher resistance to permanent deformation. To create more findings and put the presented conclusions on a stronger basis, a future test program will take into account a variation of void content, gradation type and binder type and content of mixes. The results received from this study showed a similar reduction of the creep rates for both mixes. By expanding the test program, a sensitivity analysis will be carried out to quantify the impact of different mix design parameters on the ratio of results from standard vs. enhanced TCCT. Since the enhanced TCCT takes into account the viscoelastic material reaction and thus can be expected to simulate the field performance in a more realistic way, the larger test program will provide information on which mix design parameters have the largest impact on the performance and need to be taken into consideration for efficient mix design optimization.

REFERENCES

Allen, J.J., Thompson, M.R., 1974. Resilient response of granual materials subjected to time-dependent lateral stresses. Transportation Research Record 510, 1–13.

Brown, S.F., Hyde, A.F.L., 1975. Significance of cyclic confining stress in repeated-load triaixal testing of granual material. Transportation Research Record 537, 49—58.

Clec'h, P., Sauzeat, C., Di Benedetto, H., 2009. Multidirectional behavior of bituminous mixture. In: Proceedings of Bearing Capacity of Roads, Railways, and Airfields, Chicago, 2009.

De Visscher, J., Maeck, J., Vanelstraete, A., 2006. The permanent deformation law of asphalt mixtures: investigation of the effect of mix composition and material properties. In: Proceedings of the 10th International Conference on Asphalt Pavements, Quebec, 2006.

Ebels, L., Jenkings, K., 2006. Determination of material properties of bitumen stabilised materials using tri-axial testing. In: Proceedings of the 10th International Conference on Structural Design of Asphalt Pavements, Quebec, 2006.

EN 12697-22, 2007. Bituminous Mixtures—Test Methods for Hot Mix Asphalt—Part 22: Wheel Tracking.

EN 12697-25, 2005. Bituminous Mixtures—test Methods for Hot Mix Asphalt—Part 25: Cyclic Compression Test.

EN 12697-33, 2007. Bituminous Mixtures Test Methods for Hot Mix Asphalt—Part 33: Specimen Prepared by Roller Compactor.

EN 12697-35, 2007. Bituminous Mixtures—Test Methods for Hot Mix Asphalt—Part 35: Laboratory Mixing.

Findley, W.N., Lai, J.S.Y., Onaran, K., 1989. Creep and Relaxation of Nonlinear Viscoelastic Materials. Dover Publications Inc., Mineola.

Francken, L., 1977. Permanent deformation law of bituminous road mixtures in repeated triaxial compression. In: Proceedings of the 4th International Conference on Asphalt Pavements, Ann Arbor, 1997.

Gabet, T., Di Benedetto, H., Perraton, D., et al., 2011. French wheel tracking round robin test on a polymer modified bitumen mixture. Materials and Structures 44 (6), 1031—1046.

Hoeflinger, G., 2006. Untersuchungen zur Probekoerperherstellung von Walzasphalten mit dem Walzsegmentverdichter (Master thesis). Vienna University of Technology, Vienna, Austria.

Hofko, B., 2012. Hot Mix Asphalt under Cyclic Compressive Loading. Südwestdeutscher Verlag für Hochschulschriften, Saarbrücken.

Hofko, B., Blab, R., 2010. Assessment of permanent deformation behavior of asphalt concrete by improved triaxial cyclic compression testing. In: Proceedings of the 11th International Conference on Asphalt Pavements, Nagoya, 2010.

Hunter, A.E., Airey, G.D., Collop, A.C., 2004. Influence of compaction method on asphalt mixture internal structure and mechanical properties. In: Proceedings of the 3rd Euroasphalt & Eurobitume Congress, Vienna, 2004.

Jaeger, W., 1980. Mechanisches verhalten von asphaltprobekoerpern. Publication of the Institute for Road And Railway Engineering, University of Karlsruhe, Karlsruhe.

Kappl, K., 2004. Development of New Test Methods by Modeling Traffic Load with FEM. The Evaluation of the Christian Doppler Laboratory for Performance Based Optimization of Hot Mix Asphalt, Vienna.

Krass, K., 1971. Kriechvrhalten an zylindrischen asphaltprobekoerpern. Publication of the Institute for Road And Railway Engineering, University of Karlsruhe, Karlsruhe.

Nataatmadia, A., Parkin, A.K., 1989. Characterization of granual materials for pavements. Canadian Geotechnical Journal 26, 725—730.

ON B 3580-1, 2009. Bituminous Mixtures—Material Specifications—Part 1: Asphalt Concrete—Rules for the Implementation of ÖNORM EN 13108—1.

Perraton, D., Di Benedetto, H., Sauzéat, C., et al., 2011. Rutting of bituminous mixtures: wheel tracking tests campaign analysis. Materials and Structures 44 (5), 969—986.

Rondón, H.A., Wichtmann, T., Triantafyllidis, T., et al., 2009. Comparison of cyclic triaxial behavior of unbound granular material under constant and variable confining pressure. Journal of Transportation Engineering 135 (7), 467—478.

Taherkhani, H., Collop, A., 2006. Compressive axial and triaxial testing of asphaltic mixtures. In: Proceedings of the 10th International Conference on Asphalt Pavements, Quebec, 2006.

Verstraeten, J., 1995. Bituminous material with a high resistance to flow rutting. In: Proceedings of PIARC (Permanent International Association of Road Congresses), Technical Committee on Flexible Roads, Belgium, 1995.

von der Decken, S., 1997. Triaxialversuch mit schwellendem axial- und radialdruck zur untersuchung des verformungswiderstands von asphalten. Publication of the Institute for Road Engineering, University of Brunswick, Brunswick.

Weiland, N., 1986. Verformungsverhalten von asphaltprobekörpern unter dynamischer belastung. Publication of the Institute for Road and Railway Engineering, University of Karlsruhe, Karlsruhe.

Weise, C., Wellner, F., 2008. Determination of the fatigue behavior of asphalt mixes with the triaxial test. In: Proceedings of the 4th Euroasphalt and Eurobitume Congress, Copenhagen, 2008.

Zaman, M., Chen, D., Laguros, J., 1994. Resilient moduli of granular materials. Journal of Transportation Engineering 120 (6), 967—988.